Representations of multidimensional symmetries in networks

W. G. Harter

Instituto de Fisica, Universidade Estadual de Campinas, C.P. 1170 Campinas S.P., Brazil
(Received 29 June 1973)

Physical systems that have resonances corresponding to representations of multidimension symmetry groups can be constructed from electric circuit elements. Examples involving symmetries of two four-dimensional polytopes are shown. Also a group theoretical analysis of linear constraints is described.

I. INTRODUCTION

Characters of four-dimensional cubic symmetry were calculated on computer by Birman and Chen, [1] who speculated that these representations and symmetries might possibly be associated with accidental degeneracies in some crystal lattice vibration frequencies. In the following we demonstrate some interesting realizations of these representations and degeneracies in the vibrations of certain electrical networks, and suggest what other sorts of symmetries can be visualized and treated similarly.

In fact, the vector representations given by Birman were found by Littlewood over thirty years before,[2] but it was not made clear by Littlewood whether he knew or cared about higher point symmetries, since his main concern was the study of the permutation group and its subgroups. Nevertheless, his methods are general enough to produce the characters of any one of such higher symmetries. (Higher point symmetries are effectively catalogued by the existing regular polytopes as listed in Appendix C.)

The treatment of complex symmetric networks contained below is a straightforward extension of the usual group projection techniques,[3,4] except that one must take account of the Kirchhoff current conservation constraints. A group theoretical method for deriving the constraint effects is described in Sec. II in connection with an example that can also be treated conventionally.

In Sec. III the results of the group analysis are displayed in the form of current-flow illustrations for the elementary resonances on oscillating networks having the connectivity of the four-dimensional cube and tetrahedron. The correspondence of the high degeneracies found in each case with higher symmetry representations is demonstrated.

It is apparently incorrect to claim that such analyses fill a need in circuit engineering since probably no laboratory has considered such network configurations. It is better that we simply offer the examples as interesting diversions, and the methods as solutions awaiting a problem.

II. GROUP THEORETICAL ANALYSIS OF KIRCHHOFF CONSTRAINTS

The coordinates that describe the state of internal currents in an electric network must be chosen to be independent. The twelve coordinates $\{j_1 \ldots j_{12}\}$ indicated in Fig. 1 (a) are too many, since the number of degrees of freedom of this network is seven. In general, Kirchhoff current conservation constraints reduce the number of independent coordinates of a b-branched closed network to $b - n + 1$, where n is the number of nodes or junctions.[5]

For networks that are planar like the example in Fig. 1, it is possible to choose exactly the right number of mesh loops to be the independent coordinates as is done in Fig. 1, but it is sometimes not convenient to define mesh loops for planar or especially, nonplanar networks. However if the network possesses some topological symmetry a group theoretical coordinate definition may be more convenient in either case. For example, to define coordinates for the network in Fig. 1 the irreducible representations (IR) of the cubic-octahedral group O_h characterized by Table I, are employed. Each group operator is labeled by its effect on the Cartesian coordinates $(xyz)[(y\bar{x}\bar{z})\colon x \to y, y \to -x, z \to -z]$, and, in turn, their effect on any of the 12 (nonconservative) current states $|j_n\rangle$ is obtained by inspection as shown in Eq. (1) ($|j_n\rangle$ is the state in which unit current is flowing in branch n)

$$(y\bar{x}\bar{z})|j_1\rangle = -|j_8\rangle \cdots (y\bar{x}\bar{z})|j_{12}\rangle = -|j_9\rangle. \tag{1}$$

From these are obtained orthonormal vectors of Eq. (2) that transform irreducibly as per Eq. (3):

$$|\Psi_j^\beta\rangle = \sum_n^{12} |j_n\rangle\langle j_n|\Psi_j^\beta\rangle, \tag{2}$$

$$\langle\Psi_i^\alpha|(g)|\Psi_j^\beta\rangle = \delta^{\alpha\beta}\mathfrak{D}_{ij}^{(\alpha)}(g). \tag{3}$$

(The standard procedures that accomplish this are sketched in Appendix B.)

The coefficients $\langle j_n|\Psi_j^\beta\rangle$ define currents in the diagrams of Fig. 2 and it is seen there that some IR bases conserve currents while others do not. The seven conservative bases may replace the seven mesh loops of Fig. 1(b). In fact relations like Eq. (4) are obtained by inspection of Fig. 2:

$$|l_1\rangle = \frac{3|\Psi^{A_{2g}}\rangle}{2\sqrt{3}} - \frac{(|\Psi_1^{T_{1g}}\rangle + |\Psi_2^{T_{1g}}\rangle + |\Psi_3^{T_{1g}}\rangle}{2} + \frac{2(|\Psi_1^{T_{2g}}\rangle + |\Psi_2^{T_{2g}}\rangle + |\Psi_3^{T_{2g}}\rangle}{2\sqrt{2}}. \tag{4}$$

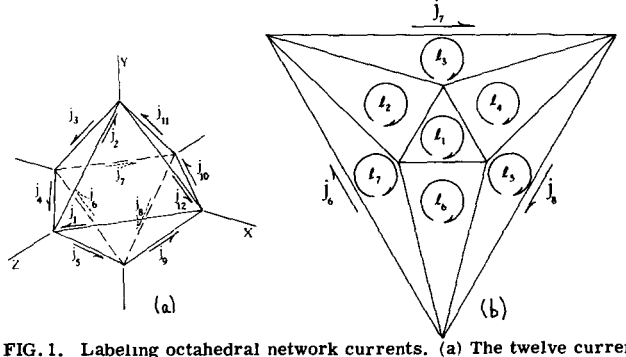

FIG. 1. Labeling octahedral network currents. (a) The twelve currents shown are not independent if conservation is required. (b) Since the network is planar, the seven mesh loops give an independent and complete labeling.

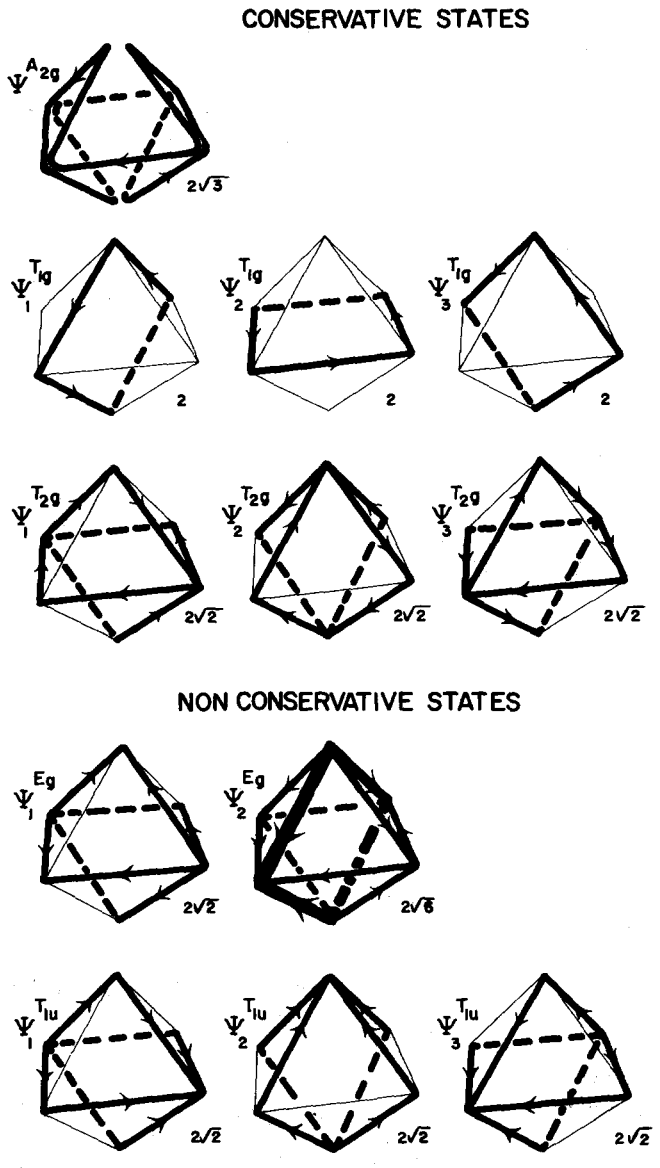

FIG. 2. Independent conservative and nonconservative states for octahedral network. Directed arrows in all configurations except Ψ_2^{Eg} represent unit current flow. Thicker arrow in the latter represents twice unit flow. Normalization denominators are shown under each figure.

A nonconservative current state will in general require all 12 states in Fig. 2 as, for example, does $|j_1\rangle$ in Eq. (5):

$$|j_1\rangle = \frac{|\Psi^{A_{2g}}\rangle}{2\sqrt{3}} - \frac{|\Psi_2^{T_{1g}}\rangle}{2} + \frac{|\Psi_1^{T_{2g}}\rangle + |\Psi_3^{T_{2g}}\rangle}{2\sqrt{2}} + \frac{|\Psi_1^{Eg}\rangle}{2\sqrt{2}} + \frac{|\Psi_2^{Eg}\rangle}{2\sqrt{6}} - \frac{(|\Psi_1^{T_{1u}}\rangle - |\Psi^{T_{1u}}\rangle)}{2\sqrt{2}}. \quad (5)$$

The question of which sets are conservative can be deduced abstractly in such a way that one can see the general results of applying symmetric linear constraints like the Kirchhoff current conservation relations.

The current conservation constraints for the octahedral network are linear in j_n and can be written in rectangular matrix form of Eq. (6), where zeroing of $c_n (n = 1, \ldots, 6)$ implies conservation:

$$\boxed{K} \begin{vmatrix} j_1 \\ j_2 \\ \cdot \\ \cdot \\ \cdot \\ j_{12} \end{vmatrix} = \begin{vmatrix} c_1 \\ c_2 \\ \cdot \\ c_6 \end{vmatrix}. \quad (6)$$

These constraints presumably have the topological symmetry of the network and this is expressed by a generalized commutation relation

$$K \cdot J(g) = C(g) \cdot K. \quad (7)$$

In the above, $J(g)$ is a 12×12 matrix that represents transformation of branch currents by group operation g of O_h following Eq. (1). $C(g)$ is an analogous 6×6 matrix that represents transformation of vertices. Both J and C are reducible, the former into $A_{2g} + T_{1g} + T_{2u} + E_g + T_{1u}$ (see Fig. 2) and the latter into $A_{1g} + E_g + T_{1u}$, and these are indicated in Eq. (8):

$$V^{-1} J V = A_{2g} + T_{1g} + T_{2u} + E_g + T_{1u},$$
$$U^{-1} C U = A_{1g} + E_g + T_{1u}. \quad (8)$$

The columns of V are the previously mentioned [Eq.

TABLE I. Character table of three-dimensional cubic octahedral symmetry group O_h. Polynomials corresponding to IR's of O_h are given.

	(xyz)	(yzx) $(y\bar{z}\bar{x})$ $(\bar{y}z\bar{x})$ $(\bar{y}\bar{z}x)$ (zxy) $(\bar{z}x\bar{y})$ $(\bar{z}\bar{x}y)$ $(z\bar{x}\bar{y})$	$(x\bar{y}\bar{z})$ $(\bar{x}y\bar{z})$ $(\bar{x}\bar{y}z)$	$(xz\bar{y})$ $(\bar{z}yx)$ $(z\bar{y}\bar{x})$ $(\bar{z}\bar{y}x)$ $(yx\bar{z})$ $(\bar{y}xz)$ $(y\bar{x}\bar{z})$ $(\bar{y}\bar{x}z)$	$(z\bar{y}x)$ $(\bar{z}yx)$ $(\bar{z}\bar{y}\bar{x})$ $(\bar{x}zy)$ $(\bar{x}\bar{z}y)$ $(x\bar{z}\bar{y})$	$(\bar{x}\bar{y}\bar{z})$	$(\bar{y}\bar{z}\bar{x})$ $(\bar{y}zx)$ $(y\bar{z}x)$ $(yz\bar{x})$ $(\bar{z}\bar{x}\bar{y})$ $(z\bar{x}y)$ $(zx\bar{y})$ $(\bar{z}xy)$	$(\bar{x}yz)$ $(x\bar{y}z)$ $(xy\bar{z})$	$(\bar{x}\bar{z}\bar{y})$ $(\bar{z}\bar{y}x)$ $(y\bar{x}\bar{z})$	$(\bar{z}y\bar{x})$ (zyx) $(\bar{y}\bar{x}z)$ (yxz) (xzy) $(x\bar{z}\bar{y})$	
A_{1g}	1	1	1	1	1	1	1	1	1	1	$x^2 + y^2 + z^2$
A_{2g}	1	1	1	−1	−1	1	1	1	−1	−1	$x^4(y^2 - z^2) + y^4(z^2 - x^2) + z^4(x^2 - y^2)$
E_g	2	−1	2	0	0	2	−1	2	0	0	$2z^2 - x^2 - y^2, \sqrt{3}(x^2 - y^2)$
T_{1g}	3	0	−1	1	−1	3	0	−1	1	−1	$y^3z - z^3y, z^3x - x^2z, x^3y - y^3x$
T_{2g}	3	0	−1	−1	1	3	0	−1	−1	1	yz, xz, xy
A_{1u}	1	1	1	1	1	−1	−1	−1	−1	−1	$x(y^3z - z^3y) + y(z^3x - x^3y) + z(x^3y - y^3x)$
A_{2u}	1	1	1	−1	−1	−1	−1	−1	1	1	xyz
E_u	2	−1	2	0	0	−2	1	−2	0	0	$\sqrt{3}xyz(x^2 - y^2), xyz(2z^2 - x^2 - y^2)$
T_{1u}	3	0	−1	1	−1	−3	0	1	−1	1	x, y, z
T_{2u}	3	0	−1	−1	1	−3	0	1	1	−1	$x(y^2 - z^2), y(z^2 - x^2), z(x^2 - y^2)$
	identity	± 120° rotation class	180° rotation class	± 90° rotation class	180° rotation class	inversion	± 120° rotation inverstion class	mirror reflection class	± 90° rotation inversion class	mirror reflection class	
				0							

(2)] current vectors $|\Psi_j^{(\alpha)}\rangle$. Now, rewritting Eq. (7) as Eq. (9) below,

$$U^{-1}K\ V\ V^{-1}\ J(g)V = U^{-1}\ C(g)\ U\ U^{-1}\ K\ V, \tag{9}$$

and applying Schur's lemmas[6] to selected block submatrices of the matrix $U^{-1}\ K\ V$, one proves that the latter must have the form:

$$U^{-1}\ K\ V = \begin{array}{c|ccccc} & \overline{A_{2g}} & T_{1g} & T_{2g} & E_g & T_{1u} \\ \hline A_{1g} & \cdot & \cdot & \cdot & \cdot & \cdot \\ E_g & \cdot & \cdot & \cdot & \alpha & \cdot \\ E_g & \cdot & \cdot & \cdot & \alpha & \cdot \\ T_{1u} & \cdot & \cdot & \cdot & \cdot & \beta \\ T_{1u} & \cdot & \cdot & \cdot & \cdot & \beta \\ T_{1u} & \cdot & \cdot & \cdot & \cdot & \beta \end{array} \tag{10}$$

Finally one obtains the following:

$$K\ V = \begin{array}{|c|c|} \hline \text{submatrix guaranteed zero} & \text{submatrix not guaranteed zero} \\ \hline \end{array} \tag{11}$$

which, if compared with Eq. (6), is seen to state explicitly that the first seven current states (Fig. 2) are conservative while the remainder may not be.

For the preceding analysis of constraints to be valuable, one only needs to know some topological symmetry of the network in question, which in turn presumably corresponds to the symmetry of the constraints. If in addition the equation of motion for transient currents in the network has this same symmetry, then the conservative IR bases (Fig. 2) will be the normal modes or elementary resonances of the network. In this latter case we can say that the physical symmetry is the same as the topological symmetry. When the physical symmetry is lower than the topological symmetry some mixing of the conservative states may be necessary to produce the resonant modes.

Also mixing will be necessary for repeated equivalent IR's should they appear in columns or rows of relations like Eq. (8). The procedures for dealing with these occurrences are straightforward.

III. EXAMPLES OF NONPLANAR NETWORKS

The cubic configuration shown in Fig. 3 has 17 conservative degrees of freedom, but it is not immediately clear how 17 independent loops could be drawn into the 32 branches. However, the IR of O_h, which correspond to conservative states, are easily found (Fig. 4). The IR's T_{1g} and E_u both appear twice, and so one is at first free to pick arbitrary orthogonal combinations of the pair of T_{1g} — IR's and similarly for the E_u.

A most interesting application of this involves finding the frequencies of normal vibration of a linear tank circuit constructed upon this network.

The equations of motion are a coupled set of 32 differential equations, the first of which is given by

$$\frac{d^2 i_1}{dt^2} = ai_1 + bi_2 - ci_3 + bi_4 + bi_5 - ci_6 + bi_7 - bI_1 + bI_7 + cj_1. \tag{12}$$

The coefficients a, b, etc. are assumed to be constants dependent upon impedance values of branches and arranged so that the *physical* symmetry is O_h.

If $b = b'$ and $c = c'$ the currents drawn in Fig. 4 are in precisely the right proportion to decouple the 32

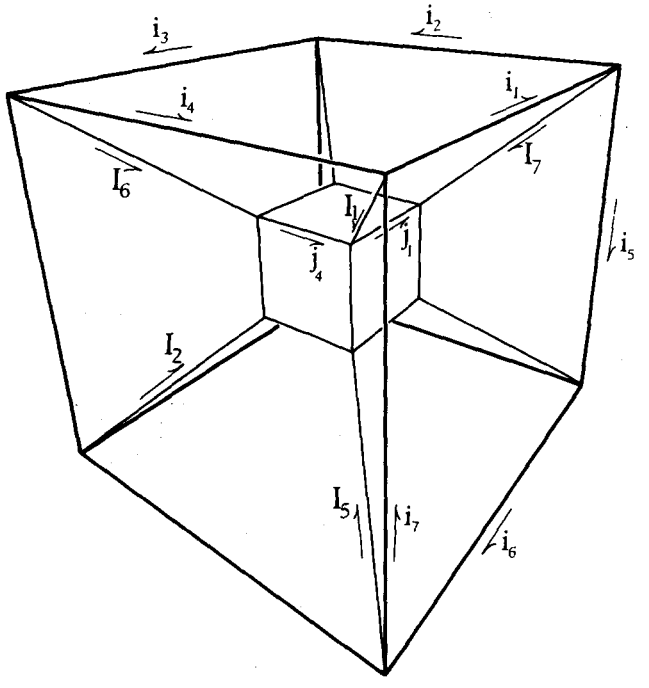

FIG. 3. Nonplanar network having cubic symmetry. The 32 currents shown are not independent. Furthermore, the mesh loop procedure successful in Fig. 1 cannot be applied here.

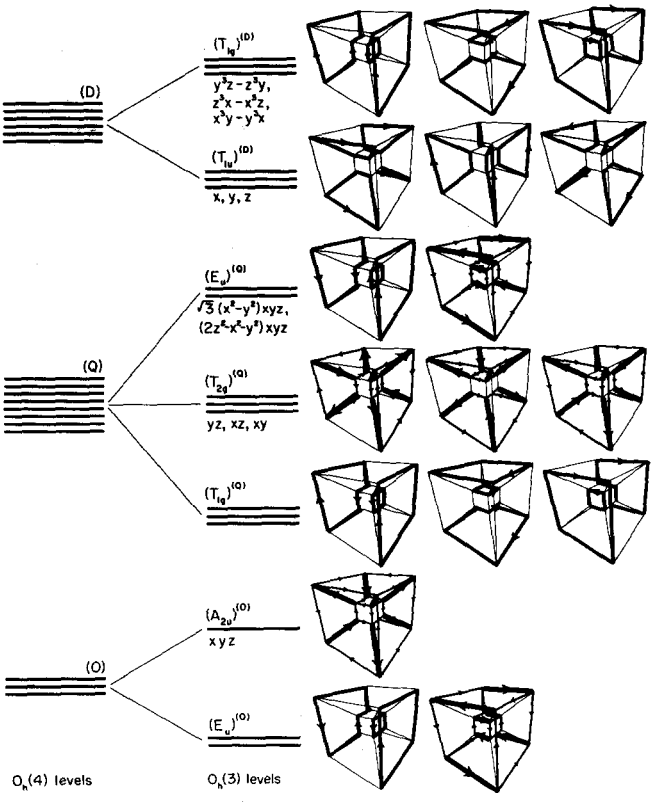

FIG. 4. Independent conservative states of cubic network and level diagrams for modes under three- and four-dimensional cubic symmetry. As shown in the text, the higher degeneracies can be traced to certain IR's of the higher symmetry.

equations of motion. The resulting equation for each of the first six modes (the D modes) is

$$\frac{d^2D}{dt^2} = (a + 2b + c)D. \tag{13}$$

The next eight modes (labeled Q modes) all satisfy another equation:

$$\frac{d^2Q}{dt^2} = (a + 2b - c)Q. \tag{14}$$

The remaining three modes have still another equation.

$$\frac{d^2O}{dt^2} = (a + 2b - 3c)O. \tag{15}$$

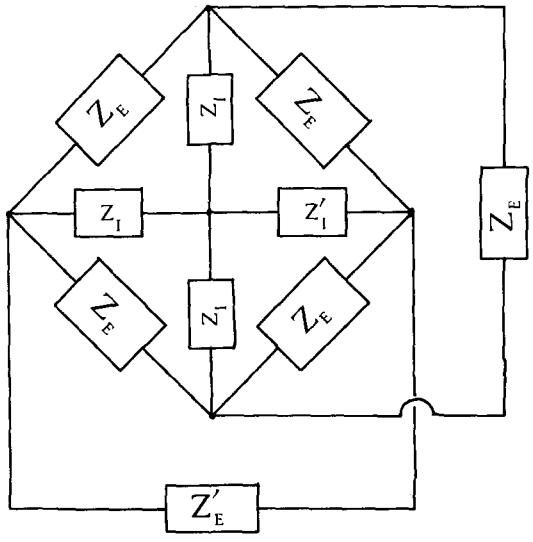

FIG. 5. Impedance bridge. Each impedance block Z_n represents series effective capacitance and inductance C_n and L_n, respectively. This is the simplest example of a nonplanar network.

The degeneracies in frequency of $(T_{1g})^{(D)}$ and $(T_{1u})^{(D)}$ at $\omega^D = \sqrt{a} + 2b + c$, of $(E_u)^{(Q)}$, $(T_{2g})_{(Q)}$, and $(T_{1g})^{(Q)}$ at $\omega^Q = \sqrt{a} + 2b - c$, and of $(A_{2u})^{(0)}$ and $(E_u)^{(0)}$ at $\omega^{(0)} = \sqrt{a} + 2b - 3c$ might seem unexpected (accidental) but one can prove that they correspond to an IR of the four-dimensional cubic octahedral group $O_h(4)$.

This is accomplished shortly after one realizes that the order of the group $O_h^{(4)}$ must be 384 (Appendix C), for there exists a subgroup of S_8 of order 384 which Littlewood has found, along with a great number of other groups that he has listed.[2] With a bit of patience one may finally sort and identify the characters and classes of Littlewood's group with this group of higher cubic symmetry. The result is tabulated below (Table II) and comparison with Table I verifies the degeneracies and splittings shown in the level diagrams of Fig. 4.

As a final example, consider the simplest nonplanar network: the well known Wheatstone bridge in Fig. 5.

The topological symmetry is S_5, which happens to be isomorphic to the four-dimensional tetrahedral symmetry. The physical symmetry of the bridge depends, of course, upon the values of the impedances, and examples varying from S_5 to S_1 are shown in Fig. 6. The IR of S_n are labeled by Young tableaux.

ACKNOWLEDGMENTS

I would like to thank John E. Heighway, Jan Smit, and Martin Gundersen for interesting conversations concerning these objects of thought.

APPENDIX A: CONSTRUCTING IR FROM POLYNOMIALS

Polynomials in $x^\alpha y^\beta z^\gamma$ that form the bases of IR of O_h are given in Table I. A norm is defined for these bases as follows:

$$\langle x^\alpha y^\beta z^\gamma | x^{\alpha'} y^{\beta'} z^{\gamma'} \rangle = \delta_{\alpha\alpha'}\delta_{\beta\beta'}\delta_{\gamma\gamma'}. \tag{A1}$$

TABLE II. The character table of four-dimensional "cubic-octahedral" symmetry $O_h(4)$.
The four-dimensional cube has eight volumes that will be permuted one into the other by the rotations of $O_h(4)$, hence the latter is isomorphic to a subgroup of S_8. Littlewood's procedure is used to derive the characters.

IR of $O_h(4)$		identity	± 120° rotations	180 rotations	± 90° rotations	180° rotations	inversion ± 120° rotation inversions	mirror reflections	± 90° rotation inversions	mirror reflections	classes of $O_h(3)$ found in $O_h(4)$ classes										$O_h(3)$ content of $O_h(4)$ IR
	A	1	1	1	1	1	1	1	1	1	1	1	1	1	1	1	1	1	1	1	A_{1g}
	B	1	1	1	−1	−1	−1	−1	1	1	1	1	1	−1	−1	−1	−1	1	1	1	A_{2u}
	C	6	0	−2	−2	2	0	0	0	0	6	0	2	−2	0	0	0	−2	0	0	$T_{2u} + T_{2g}$
	D	6	0	−2	2	−2	0	0	0	0	6	0	2	2	0	0	0	−2	0	0	$T_{1u} + T_{1g}$
	E	4	1	0	2	0	−2	1	2	0	2	−4	−1	0	−2	0	0	−1	0	0	−2 $A_{1g} + T_{1u}$
	F	4	1	0	−2	0	2	−1	−2	0	2	−4	−1	0	2	0	0	1	0	0	−2 $A_{2u} + T_{2g}$
	G	4	1	0	−2	0	−2	1	2	0	−2	−4	−1	0	2	0	0	−1	0	0	2 $A_{2g} + T_{2u}$
	H	4	1	0	2	0	2	−1	−2	0	−2	−4	−1	0	−2	0	0	1	0	0	2 $A_{1u} + T_{1g}$
	I	6	0	−2	0	0	0	0	0	−2	2	6	0	−2	0	0	0	0	2	0	2 $T_{2g} + T_{1u}$
	J	6	0	−2	0	0	0	0	0	2	−2	6	0	−2	0	0	0	0	2	0	−2 $T_{1g} + T_{2u}$
	K	2	−1	2	0	0	2	−1	2	0	0	2	−1	2	0	0	2	−1	2	0	0 E_g
	L	2	−1	2	0	0	−2	1	−2	0	0	2	−1	2	0	0	−2	1	2	0	0 E_u
	M	3	0	3	1	1	−3	0	−3	−1	−1	3	0	−1	1	−1	1	0	−1	1	−1 $A_{1u} + E_u$
	N	3	0	3	−1	−1	3	0	3	−1	−1	3	0	−1	−1	1	−1	0	−1	1	−1 $A_{2g} + E_g$
	O	3	0	3	−1	−1	−3	0	−3	1	1	3	0	−1	−1	1	1	0	−1	−1	1 $A_{2u} + E_u$
	P	3	0	3	1	1	3	0	3	1	1	3	0	−1	1	−1	−1	0	−1	−1	1 $A_{1g} + E_g$
	Q	8	−1	0	0	0	4	1	−4	0	0	−8	1	0	0	0	0	−1	0	0	0 $T_{1g} + T_{2g} + E_u$
	R	8	−1	0	0	0	−4	−1	4	0	0	−8	1	0	0	0	0	1	0	0	0 $T_{1u} + T_{2u} + E_g$
	S	1	1	1	−1	−1	1	1	1	−1	−1	1	1	1	−1	−1	−1	1	1	−1	−1 A_{2g}
	T	1	1	1	1	1	−1	−1	−1	−1	−1	1	1	1	1	1	−1	−1	−1	−1	−1 A_{1u}
Cycle structure of S_8 class		1^8	$1^2,3^2$	$1^4,2^2$	$1^4,4$	$1^2,2^3$	$1^2,2^3$	$1,6$	$1^6,2$	$1^2,2,4$	$1^4,2^2$	2^4	$2,6$	4^2	$2^2,4$	8	$2^2,4$	$2,3^2$	2^4	4^2	2^4	
Order of $O_h(4)$ class		1	32	6	12	24	4	32	4	24	12	1	32	12	12	48	24	32	12	48	12	

From this the IR matrix components $\mathfrak{D}$ follow immediately. For example, $|{}^{E_g}_{1}\rangle \equiv (|x^2\rangle - |y^2\rangle)/\sqrt{2}$, and $|{}^{E_g}_{2}\rangle \equiv (2|z^2\rangle - |x^2\rangle - |y^2\rangle)/\sqrt{6}$ are bases of IR E_g according to Table I, and of unit norm according to (A1). Then for group element (yzx) we have the following:

$$\mathfrak{D}^{E_g}_{11}(yzx) = \left\langle {}^{E_g}_{1} \middle| (yzx) \middle| {}^{E_g}_{1} \right\rangle = \left\langle {}^{E_g}_{1} \middle| (yzx) \frac{|x^2\rangle - |y^2\rangle}{\sqrt{2}} \right.$$
$$= \left\langle {}^{E_g}_{1} \middle| \frac{|y^2\rangle - |z^2\rangle}{\sqrt{2}} = -\tfrac{1}{2} \right.$$

$$\mathfrak{D}^{E_g}_{12}(yzx) = \left\langle {}^{E_g}_{1} \middle| (yzx) \middle| {}^{E_g}_{2} \right\rangle = \left\langle {}^{E_g}_{1} \middle| \frac{2|x^2\rangle - |y^2\rangle - |z^2\rangle}{\sqrt{6}} \right.$$
$$= \sqrt{3}/2$$

$$\mathfrak{D}^{E_g}_{21}(yzx) = -\sqrt{3}/2$$

$$\mathfrak{D}^{E_g}_{22}(yzx) = -\tfrac{1}{2}.$$

APPENDIX B: CONSTRUCTING IR CURRENTS

States $|\Psi_1^{(\alpha)}\rangle, |\Psi_2^{(\alpha)}\rangle, \ldots, |\Psi_l^{(\alpha)}(\alpha)\rangle$ that obey Eq. (3), and thereby comprise a normalized basis of IR (α), are found by applying projection operators $P_{1m}^{(\alpha)}, P_{2m}^{(\alpha)}, \ldots, P_l^{(\alpha)}(\alpha)_m$ defined by (B1):

$$P_{bm}^{(\alpha)} = \left(\frac{l^{(\alpha)}}{\text{number of group operators}} \right) \sum_{\substack{\text{group} \\ \text{operators} \\ g}} \mathfrak{D}_{bm}^{(\alpha)}(g)^* g \tag{B1}$$

to state vector like $|j_1\rangle$ as in (B2). (It will be assumed that vectors like $g|j_1\rangle$ span the entire space in question, which in this first case is the 12-branch octahedral network. If not, other state vectors, like $|I_1\rangle$ and $|i_1\rangle$ in the case of Fig. 3, are picked, and the process to be described here is repeated for each.)

$$P_{lm}^{(\alpha)}|j_1\rangle = N_m^{(\alpha)}|\Psi_l^{(\alpha)}\rangle. \tag{B2}$$

In (B2) the scalar $N_m^{(\alpha)}$ is either a normalization constant or zero, and is determined quickly by (B3):

$$N_m^{(\alpha)} = \langle j_1|P_{mm}^{(\alpha)}|j_1\rangle. \tag{B3}$$

For those in which $N_m^{(\alpha)} \neq 0$, exactly $l^{(\alpha)}$ orthonormal states $|\Psi_l^{(\alpha)}\rangle$ $(l = 1, 2, \ldots, l^{(\alpha)})$ are constructed according to (B2). Those m for which $N_m^{(\alpha)} = 0$ give nothing.

For example, the operators (B4) with $(\alpha) = T_{1g}$

$$P_{12}^{T_{1g}} = \tfrac{1}{16}\{(zxy) + (\bar{z}x\bar{y}) - (\bar{z}\bar{x}y) - (z\bar{x}\bar{y}) - (y\bar{x}z) + (\bar{y}xz) + (yx\bar{z}) - (\bar{x}\bar{y}\bar{z}) + (\bar{z}\bar{x}\bar{y}) + (z\bar{x}y) - (zx\bar{y}) - (\bar{z}xy) - (\bar{y}x\bar{z}) + (y\bar{x}\bar{z}) - (\bar{y}\bar{x}z) - (xyz)\},$$

$$P_{22}^{T_{1g}} = \tfrac{1}{16}\{(xyz) - (x\bar{y}\bar{z}) + (\bar{x}y\bar{z}) - (\bar{x}\bar{y}z) + (\bar{z}yx) + (zy\bar{x}) - (z\bar{y}x) - (\bar{z}\bar{y}\bar{x}) + (\bar{x}\bar{y}\bar{z}) - (\bar{x}yz) + (x\bar{y}z) - (xy\bar{z}) - (z\bar{y}\bar{x}) + (\bar{z}y\bar{x}) - (\bar{z}\bar{y}x) - (zyx)\} \tag{B4}$$

$$P_{32}^{T_{1g}} = \tfrac{1}{16}\{(yzx) - (y\bar{z}\bar{x}) + (\bar{y}z\bar{x}) - (\bar{y}\bar{z}x) + (xzy) - (x\bar{z}\bar{y}) - (\bar{x}\bar{z}\bar{y}) + (\bar{x}zy) + (\bar{y}\bar{z}\bar{x}) - (\bar{y}zx) + (y\bar{z}x) - (yz\bar{x}) + (\bar{x}\bar{z}\bar{y}) - (\bar{x}z\bar{y}) - (xzy) + (x\bar{z}\bar{y})\}$$

will give three states when applied to $|j_1\rangle$ since $N_2^{T_{1g}}$ is nonzero,

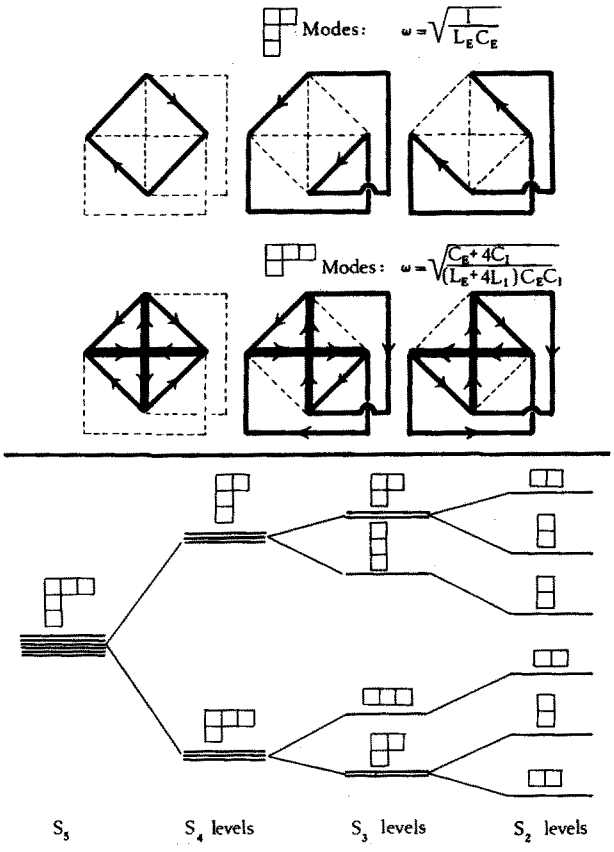

FIG. 6. Mode and frequency level diagram for various physical symmetries of bridge. Values of impedances are $S_5 \ldots Z_E = Z_E' = Z_I = Z_I'$, $S_4 \ldots Z_E' = Z_E \neq Z_I = Z_I'$, $S_3 \ldots Z_E = Z_E' \neq Z_I \neq Z_I'$, and $S_2 \ldots Z_E \neq Z_E' \neq Z_I \neq Z_I'$.

TABLE III. Characteristics of four-dimensional "regular solids."

	Vertices	Lines	Surfaces	3-Volumes	4-Volumes
"Tetrahedron"	5	10	10	5	1
"Octahedron"	8	24	32	16	1
"600 Cell"	120	720	1200	600	1
"Cube"	16	32	24	8	1
"24 Cell"	24	96	96	24	1
"Dodecahedral complex"	600	1200	0	120	1

$$\langle j_1|P_{22}|j_1\rangle = \langle j_1|\tfrac{1}{16}\{(xyz)\cdots - (z\bar{y}x)\cdots + (x\bar{y}z)\cdots - (zyx)\}|j_1\rangle = \tfrac{1}{4} = N_2^{T_{1g}}.$$

The resulting orthonormal states are given in (B5), and

$$|\Psi_1^{T_{1g}}\rangle = \frac{1}{\sqrt{N_2^{T_{1g}}}} P_{12}^{T_{1g}}|j_1\rangle = \frac{1}{2}(|j_2\rangle - |j_5\rangle + |j_8\rangle - |j_{11}\rangle),$$

$$|\Psi_2^{T_{1g}}\rangle = \frac{1}{\sqrt{N_2^{T_{1g}}}} P_{22}^{T_{1g}}|j_1\rangle = \frac{1}{2}(|j_1\rangle - |j_4\rangle + |j_7\rangle - |j_{10}\rangle), \tag{B5}$$

$$|\Psi_3^{T_{1g}}\rangle = \frac{1}{\sqrt{N_2^{T_{1g}}}} P_{32}^{T_{1g}}|j_1\rangle = \frac{1}{2}(-|j_3\rangle + |j_6\rangle - |j_9\rangle + |j_{12}\rangle)$$

drawn in Fig. 1.

The number $f^{(\alpha)}$ of independent multiplets $\{|\Psi_1^{(\alpha)}\rangle \ldots |\Psi_l^{(\alpha)}(\alpha)\rangle\} \cdots \{|\Psi_1^{(\alpha)} \cdots |\Psi_l^{(\alpha)}(\alpha)\rangle\}^{f^{(\alpha)}}$ is given by the standard frequency formula[7]:

TABLE IV. n-Dimensional "Solids."

"Tetrahedron"

n	Vertices	Lines	Surfaces	3-Volumes	4-Volumes	5-Volumes
0	1					
1	2	1				
2	3	3	1			
3	4	6	4	1		
4	5	10	10	5	1	
5	6	15	20	15	6	1
.	.	.	.	.	.	.
.	.	x	y	.	.	.
.	.	.	$x+y$	.	.	.

"Cube"

n	Vertices	Lines	Surfaces	3-Volumes	4-Volumes	5-Volumes
0	1					
1	2	1				
2	4	4	1			
3	8	12	6	1		
4	16	32	24	8	1	
5	32	80	80	40	10	1
.	.	.	.	.	.	.
.	.	x	y	.	.	.
.	.	.	$x+2y$	.	.	.

"Octahedron"

n	Vertices	Lines	Surfaces	3-Volumes	4-Volumes	5-Volumes
0	1					
1	2	1				
2	4	4	1			
3	6	12	8	1		
4	8	24	32	16	1	
5	10	40	80	80	32	1
.	.	.	.	.	.	.
.	.	x	y	.	.	.
.	.	.	$2x+y$	.	.	.

$$f^{(\alpha)} = \frac{1}{\text{number of group operators}} \sum_{\substack{\text{group} \\ \text{operators} \\ g}} \chi^{(\alpha)*}(g)\,\mathrm{Tr}J(g), \tag{B6}$$

where

$$\mathrm{Tr}J(g) = \sum_{n=1}^{12} \langle j_n | (g) | j_n \rangle.$$

In the above example $f^{T_1 g} = 1$.

APPENDIX C: GENERAL POINT SYMMETRY

There is a correspondence between a regular (Platonic) polytope and a highest point symmetry in a give Euclidian n space. The five three-dimensional regular solids are the tetrahedron having point symmetry T_d the cube and octahedron each having point symmetry O_h, and finally the icosahedron and dodecahedron having Y_h symmetry. No three-dimensional point symmetries exist outside of these except the symmetries $R(2)$ and $R(3)$ of the cylinder and sphere, respectively, and their subgroups.

Similarly the six four-dimensional regular "solids" described in Table III correspond to high four-dimensional point symmetry.

The fourth "solid" is topologically represented in Fig. 3, and has an order 384 point symmetry corresponding to all combinations of $(\pm x_1, \pm x_2, \pm x_3, \pm x_4)$.

Beyond this there are only three n-dimensional solids for any given $n \geq 5$. These are recorded in the easily remembered triangle tables given in Table IV.

[1]L. C. Chen and J. L. Birman, J. Math. Phys. 12, 2454 (1971).
[2]D. E. Littlewood, *Theory of Group Characters* (Oxford, London, 1958), p.278.
[3]E. Wigner, *Group Theory and Applications* (Academic, New York, 1959).
[4]M. Hamermesh, *Group Theory and Applications to Physical Problems* (Addison-Wesley, Reading, Mass., 1964).
[5]Steven Bose, *Network Theory* (Harper & Row, New York, 1965).
[6]Reference 3, p. 75.
[7]Reference 4, p. 104.